Anal Bioanal Chem (2010) 396:2769–2783
DOI 10.1007/s00216-009-3402-8

REVIEW

Acoustics and atomic force microscopy for the mechanical characterization of thin films

Daniele Passeri · Andrea Bettucci · Marco Rossi

Received: 31 August 2009 / Revised: 11 December 2009 / Accepted: 14 December 2009 / Published online: 13 January 2010

Abstract The science and technology of thin films require the development of nondestructive methods for their quantitative mechanical characterization with nanometric spatial resolution. High-frequency ultrasonic techniques—especially acoustic microscopy—and atomic force microscopy (AFM) have been demonstrated to represent versatile tools for developing such methods. In particular, in the last 15 years, the combination of AFM, which can probe the surface of a sample by applying ultralow loads (from micronewtons down to piconewtons) with a micromachined tip having an apex radius of a few nanometers, and ultrasonics techniques led researchers to develop some unique tools which allow one to perform not only spot measurements of the sample elastic modulus, but also to obtain both the qualitative imaging of mechanical properties and the quantitative mapping of the elastic modulus of the sample surface with nanometric lateral resolution. In the present review, firstly a brief overview of the main ultrasound-based techniques for thin film characterization is reported. Then, some of the ultrasonic AFM techniques are described, emphasizing their capability of retrieving maps of both the tip–sample contact stiffness and the sample elastic modulus. Although these techniques are less affected by the mechanical properties of the substrates than standard indentation tests, a method for the correction of the substrate effect in ultrathin films is reported in detail. Finally, by probing the mechanical properties of a small portion of the sample volume underneath the tip, we illustrate the techniques as tools for the qualitative and quantitative characterization of variations in the adhesion between a thin film and a buried interface, as well as for detecting subsurface defects, voids, cracks, and dislocations.

Keywords Atomic force microscopy · Thin film · Interface/surface analysis · Ultrasonics · Mechanical properties

D. Passeri (✉) · A. Bettucci · M. Rossi
Department of Energetics, University of Rome "La Sapienza",
Via A. Scarpa 16,
00161 Rome, Italy
e-mail: daniele.passeri@uniroma1.it

D. Passeri
Consorzio Nazionale Interuniversitario
per le Scienze Fisiche della Materia (CNISM),
Via A. Scarpa 16,
00161 Rome, Italy

Introduction

The wide number of technological applications of either inorganic or organic thin films (e.g., microelectromechanical and nanoelectromechanical systems [1]; electronic and magnetic storage devices [2–7]; chemical and biochemical sensors [2, 8, 9]; optical, optoelectronic, and photovoltaic devices [2, 7, 10, 11]; wear- and corrosion-resistant protective hard coatings [12–15], eventually also for biological applications [16]) requires the investigation of their structural, chemical and biochemical, mechanical, thermal, electrical, magnetic, and optical properties. In particular, the mechanical characterization is fundamental also for films designed for applications not directly connected with their mechanical properties, since thin-film devices may be subjected to stresses during both the realization process and routine functioning, resulting in failures or substrate-dependent lack of adhesion [17, 18]. To realize reliable devices, the characterization and the optimization of the mechanical properties of thin films is fundamental, not only with regard to Young's modulus and hardness, but also for the evaluation of inhomogeneity of

both thickness and mechanical properties, film-substrate adhesion, wear resistance, and the presence of microdefects that may dramatically reduce the lifetime of the devices [19, 20]. Consequently, for the characterization of the mechanical properties of thin films, we require the development of instruments and techniques that, from the perspective of miniaturization of devices, ensure micrometric and nanometric spatial resolution and that are nondestructive at these scales.

High-frequency ultrasonic techniques

Ultrasound-based nondestructive techniques for material testing are a well-established tool to determine the mechanical properties of a given material; moreover, since ultrasonic waves can easily penetrate opaque materials whereas many others type of radiation—such as visible light—cannot, they are being used for subsurface imaging [21]. Most such techniques have been natively developed for macroscopic specimens; therefore they utilize acoustic waves in the range approximately from 1 to 100 MHz, corresponding, in a typical solid, where the average sound velocity is 5,000 m/s, to wavelengths of 1 mm to 10 μm.

To apply such techniques for the characterizations of thin films, the frequency of the elastic waves has to be shifted to the gigahertz/terahertz range, because, for nanoscale longitudinal resolution, the wavelength of the elastic waves should also be in the nanometer range: the generation and the detection of very high frequency elastic waves, especially owing to the high attenuation they suffer, is a challenging experimental task. For example, to map subsurface structures, the pulse-transit-time method, usually called the pulse-echo method, is being extensively used in ultrasonic testing of macroscopic samples. It has recently been experimentally demonstrated that, with use of periodic piezoelectric nanostructures controlled through femtosecond optical pulses, terahertz longitudinal elastic waves—with 14-nm acoustic wavelength—can be generated and detected, giving subsurface information, such as thin film thickness, that cannot be obtained by atomic force microscopy (AFM) [22].

Although this technique allows subsurface three-dimensional imaging with nanometer resolution, it is very expensive because, as the experimental setup is similar to that of a typical pump-probe system, it requires two femtosecond lasers. On the other hand, Rayleigh waves, also called surface acoustic waves (SAWs), have been efficiently used to measure the elastic properties of thin supported films [23–25]. SAWs are a combination of a longitudinal motion and a shear motion which are coupled by the boundary surface. They can be easily generated by a laser or excited by interdigital transducers and they are well suited for surface analysis as their amplitude exhibits a frequency-dependent decay with depth: their energy is confined within a few wavelengths of the surface and the higher is the SAW frequency, more closely is their energy concentrated at the surface, so the film elastic properties have a strong influence on the propagation. The only drawback in using SAWs for evaluating the elastic properties of thin supported films is that the elastic parameters of the substrate have to be known in advance.

The acoustic microscope, a broadband scanned ultrasonic imaging system—that resembles a miniature sonar system—in which SAWs play a fundamental role in the formation of image contrast, is an excellent tool for determining the elastic constants of both isotropic and anisotropic thin films [26–28]. It is ideally suited for studying film adhesion and subsurface structures: for these reasons alone its working principle will be described in detail in the next section.

Indentation tests

Reliable well-established techniques for the mechanical characterization of both bulk samples and thin films are based on indentation tests, where a tip made of a hard material (e.g., diamond) with a well-known geometry (namely, the indenter) is pressed against the sample surface and the relation between the applied load and the consequent indentation is analyzed, either in the quasi-static or in the dynamic regime.

Depth sensing indentation (DSI) is a quasi-static technique where the indenter is pressed against and then retracted from the sample surface [29–32]. The slope of the onset of the unloading load versus indentation curve (namely, the tip-sample contact stiffness k_s) is related to the indentation modulus M_s, which for an isotropic sample is defined as $M_s = E_s/\left(1-\nu_s^2\right)$ (where E_s and ν_s are the sample Young's modulus and the Poisson ratio, respectively), whereas for an anisotropic sample it has to be numerically evaluated by the elastic tensor coefficients c_{ij} [33].

In dynamic mechanical analysis (DMA), by analyzing the amplitude and phase relations between the modulated load and the subsequent oscillating indentation, one characterizes the sample complex indentation modulus, whose real and imaginary parts (namely, the storage and loss moduli, respectively) represent its instantaneous (elastic) and delayed (viscous) responses, respectively, the former corresponding to the indentation modulus and the latter differing from zero for viscoelastic materials [34–36]. Both DSI and DMA are well-established techniques whose reliability derives from the precise control of both load and penetration as well as from the use of a tip with well-known and relatively stable shape and dimensions. In particular, since the original formulation [37–40], DSI has been and is actually being extensively investigated to take into account a number of effects (e.g., blunting of the tip [41],

viscoelasticity [42], and the presence of a substrate [43]) that were neglected in the original models. In particular, as far as thin films and coatings are concerned, several methods have been developed to evaluate the mechanical properties of the layer itself as distinct from those of the film-substrate system [44–47].

The effect of the substrate depends on the ratio between the stress at the film-substrate buried interface and that at the film surface (applied by the indenter): the lower the ratio, the smaller the effect of the substrate is expected to be. Such an effect decreases as much as the thickness of the film is high with respect to the tip-sample contact radius and to the penetration depth, the latter issue leading to the commonly accepted empirical rule that the effect of the substrate is negligible for indentation depths less than 10% of the thickness of the film [48].

Mechanical characterizations by AFM

Such considerations suggested the development of AFM-based techniques to characterize mechanical properties of both bulk samples and films by using the atomic force microscope tip as an indenter. When an AFM apparatus is used, sharper tips are involved (leading to lower contact radii) and lower loads are applied (reaching lower penetration depths). Consequently, mechanical measurements can be performed that are slightly affected by the substrate also on ultrathin films, although the use of less stable tips with not completely known geometry represents the main limitation of these techniques. Moreover, if one has an AFM apparatus, such techniques may be used for the imaging of mechanical properties of samples with nanometric lateral resolution, the latter depending on the dimensions of the tip used.

Techniques have been developed that use an AFM apparatus for acquiring load versus penetration curves, thus realizing an AFM-based DSI measurement tool [49]. Since in such techniques the load is applied by the cantilever, only mechanical characterization of compliant samples is allowed (such as polymers or biologic materials) since, for stiff materials, the cantilever instead of indenting the sample surface is more easily deflected by it.

Dynamic AFM techniques

A second approach is based on the detection of the cantilever response when the load is modulated (e.g., by setting into vibration the cantilever itself or the surface of the sample, the latter by modulating the extension of the piezoelectric actuator under the sample) at frequencies above the cutoff frequency of the AFM feedback circuit, to avoid both the partial compensation of cantilever vibrations and the influence of oscillations on the AFM standard topographic images. At high frequencies, far from its resonances, the cantilever may be considered dynamically rigid. Thus, the oscillation of the sample surface results in the indentation of the surface itself by the atomic force microscope tip more than in the deflection of the cantilever. Since the modulation of the load results in a modulation of the penetration depth into the sample, the vertical interaction between the atomic force microscope tip and the sample surface can be modeled by a spring, whose elastic constant is the tip-sample contact stiffness k_s. For low modulation frequencies, indentation of the sample is achieved only if relatively stiff cantilevers (i.e., cantilevers with high spring constant k_c) are used. On the other hand, if the tip-sample contact is much stiffer than the cantilever, the tip does not indent the sample surface and the displacement of the surface produces a cantilever deflection of the same amount [50, 51]. The former operating conditions are those typically involved in the technique referred to as force-modulation microscopy [50–52].

Ultrasonic AFM techniques

At high modulation frequencies, i.e. from tens of kilohertz to a few megahertz, the cantilever dynamic stiffness is increased and the oscillation of the sample surface results in an oscillating indentation of the latter, independently of the static value of k_c. Consequently, hybrid techniques which combine ultrasonic and AFM methods represent powerful tools for the local characterization and imaging of the mechanical properties of samples, in particular of thin films. For these latter samples, the low applicable loads and the low tip curvature radii involved allow one to perform measurexments that are less affected by the substrate properties, with increased spatial resolution (which is a critical issue in the case of nanostructured materials), and that are less invasive than those performed by standard DSI and DMA techniques.

Different techniques have been developed by combing acoustics and AFM methods that allow one to retrieve, simultaneously to standard morphological characterization, images reflecting mechanical or structural properties of the samples. As an example, with use of scanning near-field ultrasonic holography, images have been obtained that reflect the structural properties of samples not evidenced by the morphological characterization, and buried structures underneath the surfaces have been visualized with nanometric resolution [53, 54]. Moreover, ultrasonic AFM (U-AFM) techniques have been developed that allow both qualitative and quantitative measurement of the local value of the contact stiffness and its mapping over the surface, thus finally characterizing the elastic modulus of the sample. In such techniques, k_s is deduced by analyzing either the linear or the nonlinear response of the cantilever excited at ultrasonic frequencies, the tip of which is in contact with the sample surface.

The linear response of the sample-tip-cantilever oscillating system is analyzed by the so-called scanning local acceleration microscopy (SLAM) [55–57] and atomic force acoustic microscopy (AFAM) [58–63] techniques (which use the same experimental setup and similar approaches for the analysis of experimental data, but they are referred to by two different names because they were developed independently), whereas the nonlinear response is analyzed by the so-called ultrasonic force microscopy (UFM) technique [64–68]. SLAM/AFAM and UFM are the most reported ultrasound-based AFM techniques which have been demonstrated to allow the reliable quantitative characterization of mechanical properties at the nanoscale. In this review, such techniques are described, with particular attention being given to the required modifications to standard AFM, to the experimental procedure, and to the data processing to obtain the local value of the contact stiffness and its mapping over the sample surface. Note that such a review is explicitly intended to provide researchers dealing with the technology of hard thin films and coatings with an overview of techniques for the quantitative mechanical characterization at the nanoscale that do not require substantial modifications to a standard AFM apparatus and, thus, they are easy to approach and to implement (also not being particularly expensive) for researchers with expertise in scanning probe microscopy.

In the following, firstly acoustic microscopy will be briefly described; then the U-AFM experimental techniques for the evaluation of the tip-sample contact stiffness k_s using SLAM, AFAM, and UFM are reported. The procedure for determining the indentation modulus of the sample, which is the same for all the techniques [37–40], is then described after the local value of k_s has been obtained and eventually mapped over the sample surface using one of the techniques. Examples of applications are reported. As regards thin films, the measured indentation modulus is affected by the mechanical properties of the substrate itself: consequently, experimental approaches are described for evaluating the elastic properties of the film as distinct from those of the film-substrate system. Finally, other structural and mechanical properties different from the mere indentation modulus are illustrated which affect the measured value of the contact stiffness: U-AFM techniques are thus demonstrated to allow also the qualitative and quantitative visualization of subsurface defects, buried structures, and inhomogeneity in the film-substrate adhesion.

Acoustic microscopy

The heart of the acoustic microscope is the acoustic lens, made of sapphire (Fig. 1) [26]. A radio-frequency tone burst containing a single radio frequency excites a piezoelectric transducer at the top of the lens, which generates an ultrasonic plane wave propagating along the lens toward the surface of a spherical cavity that has been carefully ground and polished in the lens body. A liquid is necessary between the lens and the sample to transmit the acoustic wave: water is the most frequent choice. Owing to the acoustic velocity mismatch between sapphire and water [the velocity of elastic waves in sapphire is 11,000 m/s, whereas in water it is 1,500 m/s: this means that there is a very great refractive index ($n \cong 7.4$) for the wave striking the cavity], plane waves crossing the sapphire-water interface will be refracted into spherical waves converging onto the focal point of the lens, which is generally placed beneath the sample surface.

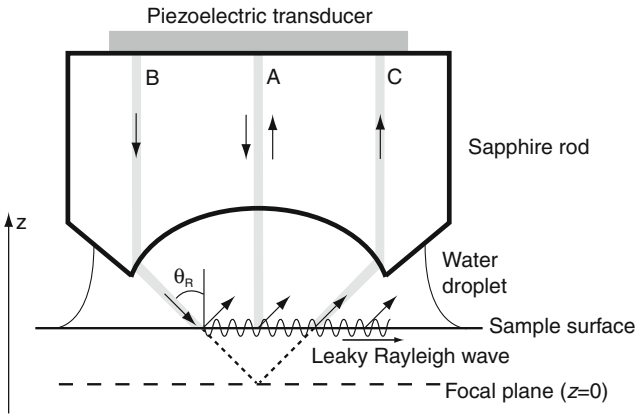

Fig. 1 The acoustic lens and the simplified ray model to show the physical origin of $V(z)$

For a simple ray model [69], the normal ray A is reflected by the sample surface toward the transducer but if the aperture of the lens is wide enough, a Rayleigh wave can be excited propagating along the sample surface: that happens for rays, such as ray B, incident at a Rayleigh angle θ_R given by Snell's law $\sin \theta_R = v_F = v_R$, where v_F is the velocity in the fluid and v_R is the Rayleigh velocity (which depends on the Poisson ratio of the sample material). Because the surface of the sample is in contact with the fluid, while propagating, the Rayleigh wave leaks energy into the fluid, generating longitudinal waves propagating (at the Rayleigh angle) toward the lens, where, therefore, ray C, symmetrically placed with respect to the incident ray B, travels back to the transducer. It can be easily understood that the electrical signal V from the ultrasonic transducer—now acting as a receiver—is due to the interference between the acoustic wave directly reflected from the sample surface and the wave that travels at the Rayleigh angle: the phase difference between the two waves is a function of the defocus z (by convention $z=0$ refers to the focal plane of the lens). Consequently, there is an interference pattern in $V(z)$ depending on the lens-to-sample

distance. The spacing between minima in $V(z)$ is related to the velocity of the Rayleigh wave and, in turn, to the elastic properties of the sample surface. Images, that qualitatively reflect the variations of the elastic constants over the surface of the sample are obtained by scanning progressively the surface and measuring in each point for a given value of z the amplitude of V. Owing to the nature of elastic waves, the acoustic microscope can be used to detect and to image defects and other subsurface structures as well as to characterize film adhesion [28, 70].

A quantitative application of the acoustic microscope is the development of line focus acoustic microscopy (LFAM) for directional measurements, where the spherical acoustic lens is substituted by a cylindrical one: it is no longer possible to obtain images, but the $V(z)$ interference pattern remains the same, with the important difference that the generated wave modes propagate in a specific direction, namely, normal to the focal line, and thus it is possible to measure velocities—and hence elastic constants—in anisotropic elastic materials, where the direction of the wave energy is not always parallel to the k-vector [71]. In particular, Achenbach et al. [72] have used LFAM to determine the elastic constants of anisotropic films deposited on anisotropic substrates. The technique is based on an inversion procedure in which best estimates of the elastic constant are put in a theoretical model of $V(z)$ to calculate the velocities and the amplitude of the leaky Rayleigh wave; these are then compared with the experimentally measured values. The difference is used to adjust the elastic constants and the process is repeated until convergence by the least-squares method is obtained. It is worthwhile noting that LFAM can detect the presence of stress between a thin film and the substrate, and in the thin film itself as stress modifies sound velocity through third-order elastic constants [73]. The only drawback of the acoustic microscope is the presence of liquid between the acoustic lens and the sample surface, which, in some cases, could change the chemical characteristic of the latter.

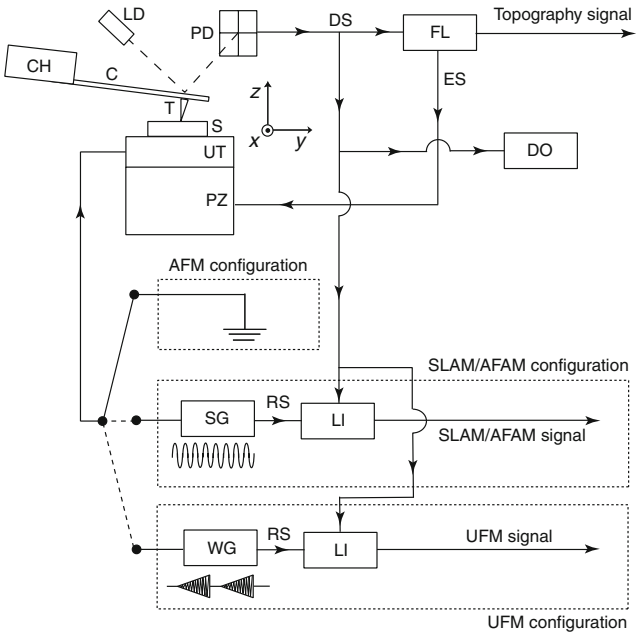

Fig. 2 The standard atomic force microscopy (*AFM*) apparatus with the modifications for either scanning local acceleration microscopy (*SLAM*)/ atomic force acoustic microscopy (*AFAM*) or ultrasonic force microscopy (*UFM*). The tip (*T*), placed at the end of the cantilever (*C*), whose other end is clamped to the cantilever holder (*CH*), is in contact with the surface of the sample (*S*). The cantilever deflection is monitored by the light beam generated by a laser diode (*LD*), which is reflected at the end of the cantilever and is detected by a four-segment photodiode (*PD*). The resulting deflection signal (*DS*) is sent as an input to the feedback loop (*FL*), which maintains constant the cantilever deflection by controlling through the error signal (*ES*) the extension of the *z*-axis piezoelectric actuator (*PZ*) and supplies the signal for the reconstruction of the sample topography. For ultrasonic AFM experiments, the sample is coupled with an ultrasonic transducer (*UT*) which is controlled either by a sinusoidal signal supplied by a signal generator (*SG*) for SLAM/AFAM or by a ramped sinusoidal wave supplied by a wave function generator (*WG*) for UFM. In both configurations, the AC component of DS, eventually visualized by a digital oscilloscope (*DO*), is analyzed by a lock-in amplifier (*LI*), synchronized by the reference signal (*RS*) from SG or WG, thus obtaining either the SLAM/AFAM or the UFM signal

Acoustic AFM-based techniques

The quantitative AFM-based acoustic techniques described in this review are generally implemented by slightly modifying a standard AFM apparatus. Although different hardware and software modifications are required for each technique, some of them may nevertheless be recognized to be common for both SLAM/AFAM and UFM. The standard AFM experimental setup with both SLAM/AFAM and UFM major modifications is sketched in Fig. 2. In particular, the feedback loop of the atomic force microscope is used to maintain the cantilever in contact, with constant deflection, with the surface of the sample. The latter is placed on, and acoustically coupled with, a piezoelectric transducer which excites acoustic vibrations at ultrasonic frequency, resulting in the out-of-plane oscillation of the sample surface and thus in the modulation of the indentation of the tip into the surface itself.

Different experimental configurations have been proposed and compared, where the ultrasonic oscillation into the sample is excited through the tip, either by coupling the cantilever chip with the piezoelectric transducer (or by using the transducer itself, which sets into vibration the cantilever in standard AFM semicontact mode) [57, 60, 74–76] or by electromechanically exciting the cantilever itself by the depletion-layer actuation method [77]. Such configurations have some practical advantages since they do not require one to access the back of the sample. They allow

the use of standard AFM setups, avoiding the contamination by acoustic coupling agents, and—in case of linear techniques—they allow one to discriminate and eventually reduce the presence of spurious peaks in the acquired vibration spectra due to resonances of the chip itself which excite forced cantilever oscillations [78]. Nevertheless, such experimental details are unessential to understand the techniques described and far exceed the aims of this review. Consequently, in the following only the "basic" configuration (oscillations excited by the piezoelectric transducer coupled under the sample) will be referred to. Finally, all the techniques require an acquisition system (generally based on lock-in techniques) to retrieve the ultrasonic signal from the detected cantilever deflection signal.

Linear techniques for contact stiffness measurement

In linear techniques (i.e., SLAM/AFAM), k_s is indirectly deduced by analyzing the flexural resonance frequencies of the atomic force microscope cantilever oscillating in the linear regime in contact with the sample surface. Figure 2 shows a block diagram of the experimental apparatus for the SLAM/AFAM technique. More details about the instrumentation and the electronic implementation can be found elsewhere [75, 79, 80]. Briefly, the piezoelectric transducer under the sample is driven by a signal generator that produces a continuous sinusoidal wave at ultrasonic frequency ω which excites an out-of-plane oscillation of the sample surface and sets into vibration the cantilever, thus resulting in the superimposition of AC components on the cantilever deflection signal. Although the tip-sample interaction is generally nonlinear, for a low vibration amplitude of the sample surface the whole system may be considered to be oscillating linearly [81]. The AC component at frequency ω of the cantilever deflection signal (not suppressed by the AFM feedback loop since it exceeds its cutoff frequency) is filtered by a lock-in amplifier, synchronized with the signal generator. By sweeping the excitation frequency ω, one acquires a linear vibration spectrum where resonance frequencies are observable corresponding either to the flexural modes of the cantilever (which are directly excited) or to the torsional ones (not directly excited, but resulting from the coupling between torsional and flexural modes due to geometrical asymmetries of the cantilever or of the tip-sample contact) [82–84]. To obtain the value of k_s, the linear spectra have to be analyzed by assuming a suitable model of the oscillating system. In particular, k_s can be deduced by comparing the measured set of contact resonance frequencies (CRFs) f_n of the flexural modes of the cantilever contacting the sample surface to the set $f_{0,n}$ of flexural resonance frequencies of the cantilever oscillating out of contact with the sample surface (where the subscript n refers to the nth flexural mode of the cantilever oscillating either out of contact or in contact with sample surface).

The simplest description of the oscillating system is the point mass model sketched in Fig. 3a. The whole cantilever is described as a concentrated mass m_c coupled to a fixed support by the parallel circuit between a spring k_c (the cantilever spring constant) and a dashpot γ_c (representing the damping of the beam and the surrounding medium, generally air). When the apex of the atomic force microscope tip is in contact with the sample surface, the normal tip-sample coupling is modeled by the parallel circuit between k_s and the contact damping γ_s. According to such a model, k_s can be calculated from the measured values of f_1 and $f_{0,1}$ through the relation [58]

$$\frac{k_s}{k_c} = \left(\frac{f_1}{f_{0,1}}\right)^2 - 1. \quad (1)$$

Note that only one resonance is predicted for the cantilever, both in the free-end case and in the spring-

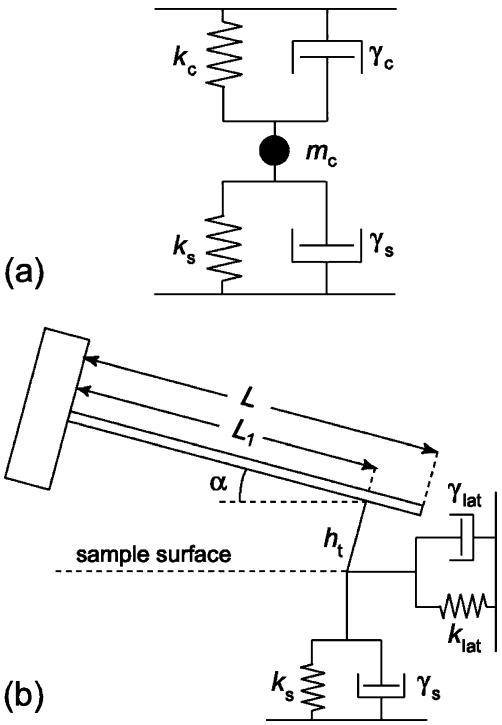

Fig. 3 **a** The point-mass model: the cantilever is described by a concentrated mass (m_c) coupled to the fixed support by the parallel circuit between the cantilever spring constant (k_c) and a dashpot (γ_c) and the tip-sample contact is modeled by the parallel circuit between the contact stiffness (k_s) and a dashpot (γ_s). **b** The beam model: the cantilever is modeled by a rectangular uniform beam with length L, clamped at one end, and inclined of an angle α with respect to sample surface. The tip, with height h_t, is supposed to be placed a distance L_1 from the cantilever clamped end. The tip-sample normal interaction is described by the parallel circuit between the contact stiffness (k_s) and a dashpot (γ_s), whereas the lateral interaction is described by the parallel circuit between the lateral stiffness (k_{lat}) and a dashpot (γ_{lat})

coupled case [58]. Several flexural and torsional modes are generally clearly visible in the resonance spectrum of the cantilever, thus indicating that the latter behaves more like a massive beam than a concentrated mass [57, 58].

A more realistic model of the cantilever in contact with the sample surface is reported in Fig. 3b. The cantilever is modeled as a beam with uniform rectangular cross section, with length L, width w, and thickness t. Although rectangular cantilevers require simpler models which may be solved analytically [58, 85], other types of cantilever may be used, such as dagger-shaped [63, 86] and V-shaped [87] ones, which nevertheless have to be described by more complicated models that may be solved by power-series or finite-element-analysis methods. According to the model sketched in Fig. 3b, the cantilever is supposed to be inclined by an angle α with respect to the sample surface. The tip, with height h_t, is supposed to be placed at a distance L_1 from the cantilever end clamped to the holder, thus allowing one to define the ratio $r=L_1/L$. More comprehensive models have been proposed which consider, for example, the tip to have a mass m_t and an arbitrary shape which determines the center of mass [84], or a not infinitely stiff clamped end cantilever [57, 78]. The normal and the lateral interactions between the tip and the sample are modeled by the parallel circuit between a linear spring k_s and a dashpot γ_s and by the parallel circuit between a linear spring (lateral contact stiffness k_{lat}) and a dashpot γ_{lat}, respectively. If k_s, γ_s, k_{lat}, and γ_{lat} are supposed to be zero, the model describes the cantilever free of oscillating out of contact with the sample surface. The model depicted can be analytically solved, thus obtaining the characteristic equation of the flexural vibration of the system [57, 58, 84, 88]. Such an equation relates the resonance frequencies of the flexural modes of the cantilevers to the parameters indicated in Fig. 3b. The solution of the system allows one to evaluate k_s from the acquired experimental resonance spectra of the cantilever. To this aim, different approaches can be followed.

According to the approach reported by Dupas et al. [57] and indicated by the authors as the SLAM technique, the whole spectrum of the cantilever is acquired in a frequency range from tens of kilohertz to a few megahertz where about ten resonances are visible, owing to the low value of k_c of the cantilever used. In the first step of the experimental procedure, the spectrum of the cantilever oscillation is acquired with the tip out of contact with the sample surface and is used to adjust the geometrical parameters of the cantilever (and eventually the stiffness at the not ideal clamped end) to optimize the agreement between the simulated and the experimental spectra [57]. The geometrical parameters of the cantilever are not independent, being related to k_c by a relation which represents a further condition to be satisfied, being that k_c is measurable by an independent method such as that of Senden and Ducker [89], Cleveland et al. [90], or Sader et al. [91]. In the second step of the experimental procedure, the tip is brought into contact with the sample surface and the spectrum of the cantilever oscillation is acquired and used to adjust the remaining parameters in Fig. 3b and, in particular, k_s [57]. Owing to the number of parameters involved, a good adjustment may be difficult to achieve, especially if too few modes are visible in the experimental spectra: consequently, the use of a soft cantilever which enables the detection of several resonances in the transducer bandwidth should be recommended.

We point out that to improve the reliability of the adjustment, experimental torsional spectra of the cantilever could be acquired (together with the flexural spectra with which we have been concerned up to here) and the parameters of the model could be adjusted to fit simultaneously both the flexural and the torsional spectra. To the best of our knowledge, such an improvement has not yet been exploited and is here suggested for further research.

A second approach, firstly proposed by Rabe et al. [58] referring to it as AFAM, takes advantage of the use of a simplified version of the model depicted in Fig. 3b. In the original works [58, 60–62], the cantilever angle α was assumed to be known (generally $\alpha=0$) and the contact was modeled by the only k_s. In such a condition, from the characteristic equation of the cantilever in contact with the sample surface, the analytical expression of k_s is obtained as a function of the nth CRF f_n and of the unknown parameter r, i.e., $k_s=k_s(f_n,r)$, these being the required geometrical parameters deduced from the measured set of free resonance frequencies $f_{0,n}$ experimentally determined with the cantilever out of contact with the sample surface [58, 61]. After the values of two CRFs, generally the first and the second (f_1 and f_2, respectively), have been acquired instead of the whole spectrum, r and k_s are calculated by imposing the relation [61, 62]

$$k_s(f_1, r) = k_s(f_2, r). \tag{2}$$

AFAM measurements reported in literature have been generally performed on stiff samples to avoid the effect of viscoelastic damping: stiff cantilevers are thus required to operate in k_s/k_c ranges below the saturation of the frequency shift and, moreover, to apply normal loads high enough to neglect the effect of adhesion.

In such conditions, in the frequency ranges investigated (up to a few megahertz) only the first and second (rarely the third) contact modes are visible. In principle, other couples of modes may be used instead of the first and the second one. As observed by Rabe et al. [60], different values of k_s are determined from different couples of frequencies and such values can be used to calculate the experimental error

in the determination of k_s itself, generally as high as 10–20% [60, 92]. Nevertheless, as described in the following, the value of k_s measured on the investigated sample has to be compared with that measured on a material with known mechanical properties used as a reference using the same tip. We found that such a ratio is rather independent of the couple of frequencies chosen for the calculation, its uncertainty being about 1 order of magnitude lower than that of k_s [92]. Consequently, the use of only f_1 and f_2 does not represent a significant limitation for the accuracy of the technique, adding only a minor uncertainty in the subsequent data processing. Finally, the extension of the AFAM technique has recently been reported for the measurement of both k_s and k_{lat} which allows one to independently evaluate the sample Young's modulus and Poisson ratio, instead of only the indentation modulus [93]. Moreover, Yuya et al. [85] recently demonstrated the capability of the AFAM technique to measure both k_s and γ_s of viscoelastic materials, thus allowing one to obtain the sample storage and loss moduli.

Nonlinear techniques for contact stiffness measurement

In the UFM technique [64–66], the experimental apparatus for which is sketched in Fig. 2, the nonlinear response of the cantilever is analyzed when the oscillation amplitude of the piezoelectric transducer underneath the sample is linearly ramped, thus exploiting the nonlinear region tip-sample interaction. Figure 4a shows a schematic representation of the force F versus indentation depth h relation, where plastic effects are neglected. Note that such a dependence should not be confused with the more familiar AFM force versus distance curves, but is deduced from the latter as reported in the literature [94]. For a certain set point value of the force (i.e., of the static cantilever deflection) F_{sp1} and thus of the indentation h_{sp1}, if the oscillation amplitude Δh of the indentation is lower than the difference h_{sp1} - h_{po} between h_{sp1} and the pull-off point h_{po}, the average normal force is still F_{sp1} and no variation in the cantilever static deflection is observed. When Δh reaches the pull-off point (i.e., for the threshold amplitude $A_1 = h_{sp1} - h_{po}$), a discontinuity of the normal force and thus of the cantilever static deflection occurs. Any further increase of Δh results in an increase of the average normal force and of the cantilever deflection [64, 65]. Consequently, the typical UFM waveform of the cantilever static deflection is obtained, which is a periodic signal whose fundamental period is the same as that of the ramp-modulated envelope of the ultrasonic piezoelectric oscillation signal. The UFM cantilever deflection signal can be visualized by an oscilloscope, thus allowing one to evaluate the threshold amplitude A_1, i.e., the value that is assumed by the ramped electric signal when the jump of the cantilever deflection occurs [64, 65]. Alternatively, the deflection signal can be analyzed by a lock-in amplifier that supplies the amplitude of its harmonic component at the repetition frequency of the linear ramp signal, which is inversely proportional to A_1 [66].

The quantitative evaluation of k_s was demonstrated by Dinelli et al. [65] through the so-called differential UFM (d-UFM) technique: referring to Fig. 4a, the UFM experiment is repeated for a second value of normal force F_{sp2} (and thus of static indentation h_{sp2}) and the corresponding threshold amplitude A_2 is obtained, allowing one to evaluate the contact stiffness as [65]

$$k_s = \frac{F_{sp2} - F_{sp1}}{A_2 - A_1}. \quad (3)$$

Note that, to evaluate k_s, the threshold amplitude has to be converted into nanometers, i.e., calibration has to be

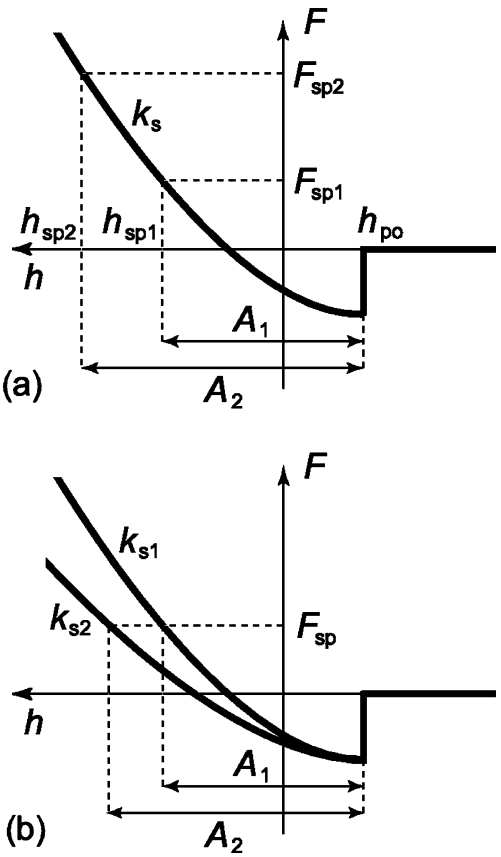

Fig. 4 **a** The force F versus indentation h curve, whose slope is the contact stiffness k_s. Two different set point forces (F_{sp1} and F_{sp2}, respectively) and the corresponding set point indentations (h_{sp1} and h_{sp2}, respectively) are indicated, together with the ultrasonic threshold amplitudes (A_1 and A_2, respectively) needed to reach the pull-off point h_{po}. **b** Two force versus indentation curves corresponding to materials with different stiffness (k_{s1} and k_{s2}, respectively, with $k_{s1} > k_{s2}$) and the same adhesion force with the tip. For the same set point force F_{sp}, the ultrasonic threshold amplitudes (A_1 and A_2, respectively) are inversely proportional to the contact stiffness

performed to relate the linearly ramped electric driving signal to the effective displacement of the transducer [64, 65]. As a general rule, calibration can be performed by measuring the threshold amplitude corresponding to several increasing values of the normal load [95, 96]. Differently from linear techniques, where k_s is indirectly obtained from the measured CRF values, UFM allows one to directly evaluate the contact stiffness, thus not requiring one to assume and to solve complicated models.

As will be described in the following, the calibration of the displacement of the piezoelectric transducer is not strictly required if UFM measurements are repeated on a reference sample, with the indentation modulus of the sample investigated being directly evaluated by comparing the slope of the force versus the uncalibrated threshold amplitude obtained on the sample investigated with that measured on the reference.

Evaluation of the sample indentation modulus

The local value of k_s of the sample surface is related to the mechanical properties of the latter, i.e., to its reduced Young's modulus E_s^*, which is defined by the relation

$$E_s^* = \left(\frac{1}{M_s} + \frac{1}{M_t}\right)^{-1}, \tag{4}$$

where M_s and M_t are the indentation moduli of the sample and the atomic force microscope tip, respectively. In particular, the value of E_s^* can be deduced from that of k_s through the relation [38–40]

$$E_s^* = \frac{k_s}{2a}, \tag{5}$$

which is valid for any axisymmetric tip, where a is the tip-sample contact radius, which is generally unknown and depends on the geometry of the tip. In particular, a can be determined by investigating the tip apex by an independent technique (e.g., by scanning electron microscopy or by AFM blind tip reconstruction using a sample with known morphology [97]) or through calibration performed by contact stiffness measurement on a sample with well-known mechanical properties used as a reference [98, 99]. In the latter case, the explicit determination of a is not strictly required, since E_s^* can be evaluated by the relation

$$E_s^* = E_r^* \left(\frac{k_s}{k_r}\right)^n, \tag{6}$$

where k_r is the tip-sample contact stiffness measured on the reference sample, E_r^* is its reduced Young's modulus (known from the literature or measured by an independent technique), and n is a geometrical parameter which depends on the shape of the atomic force microscope tip, e.g., $n=1$ or $n=3/2$ in the two particular cases of an ideally flat tip or a parabolical tip, respectively, whereas n is expected to assume intermediate values in the case of real blunt tips. Note that in the case of UFM measurements, the use of Eq. 6 does not require the explicit calibration of the piezoelectric transducer displacement. If the shape of the tip and thus n are unknown, E_s^* can be evaluated by averaging its values obtained for $n=1$ and $n=3/2$, although such an approach increases the final uncertainty in the evaluation of M_s. Alternatively, k_s can be measured for increasing values of the static normal load F_N applied by the cantilever on the sample surface, evaluated as $F_N=k_c\delta$, where δ is the cantilever static deflection [65, 81, 98, 99]. In case of a flat punch k_s is not dependent on F_N, whereas in case of a parabolical tip $k_s \propto \sqrt[3]{F_N}$.

Kopycinska et al. [100] recently proposed a generalized relation to be used to fit the k_s versus F_N experimental data to obtain the value of n. After E_s^* has been obtained by Eq. 6, M_s is obtained by Eq. 4 if the mechanical properties of the tip are known. If M_t is not known, e.g., in the case of coated tips or when wear-induced amorphization modifies the indentation modulus of the atomic force microscope silicon tip apex, the use of two reference samples is required to retrieve both M_s and M_t [101]. In general, calibration of the tip could be performed by using a set of reference samples. Finally, it is worth noting that by only measurement of k_s, only M_s can be determined, E_s and ν not being independently determinable. Conversely, if the technique used allows also one to retrieve k_{lat}, the sample shear modulus (and thus both E_s and ν) can be determined through relations for the lateral contact mechanics analogous to those used for the vertical one, as recently reported by Hurley and Turner [93].

Mechanical imaging

U-AFM techniques allow one to evaluate k_s at the tip-sample contact point, the lateral resolution depending on the tip-sample contact radius a. If the experiment is repeated and the required data are collected at each point of the surface investigated simultaneously to morphological characterization, the contact stiffness map $k_s(x,y)$ can be obtained, where x and y are the coordinates of the pixels of the scanned area. To that aim, according to the SLAM approach, the acquisition of the cantilever vibration spectrum and the adjustment of the corresponding parameters in the postexperiment data analysis are required, the whole procedure being rather time-consuming. Consequently, the SLAM approach is very effective for reliable quantitative spot measurements of k_s since it takes advantage of a rather realistic model of the cantilever, but

it is not recommended for mapping of quantitative mechanical properties, being too time-consuming.

In contrast, since the acquisition of only the f_1 and f_2 values is required to determine k_s, the AFAM approach is suitable for the quantitative mapping of the mechanical properties of the surface of samples: simultaneously to AFM standard topography, both the first and the second CRF can be acquired at each point of the scanned area (note that, depending on the experimental apparatus, two subsequent scans of the same area may be required). The contrast in such images qualitatively reflects the mechanical properties of sample surface, i.e., the higher is the resonance frequency, the stiffer is the sample. Moreover, the frequency values reported in the two CRF images can be used to solve Eq. 2 at each point of the scanned area, thus obtaining the map of $k_s(x,y)$ of the sample surface investigated [102]. The AFAM technique is consequently a powerful tool for the quantitative imaging of sample mechanical properties at the nanoscale, although its reliability depends on the suitability of the mechanical model used for the cantilever and for the contact for the particular sample under investigation, which consequently have to be carefully verified. After $k_s(x,y)$ maps have been obtained, at each point of the scanned area the value of M_s can be evaluated from that of k_s, thus reconstructing the quantitative indentation modulus map $M_s(x,y)$ of the surface. To this aim, either an external material or a portion of the imaged area of the surface itself which corresponds to a material with known mechanical properties can be used as the reference.

Finally, the SLAM/AFAM technique can be used for less time-consuming qualitative mechanical imaging. Acoustic images are acquired by driving the piezoelectric transducer using a constant value of the excitation frequency (which has to be chosen slightly above or below the first CRF, i.e., roughly in the middle of one of the halves of the resonance curve) and the cantilever oscillation amplitude value is acquired at each point of the scanned area. If the ultrasonic frequency is chosen slightly higher than f_1, when a stiffer point is probed, the local value of f_1 increases and thus the recorded amplitude increases. Consequently, the contrast in the amplitude image qualitatively reflects the variation of the mechanical properties of the surface, since brighter areas correspond to stiffer regions of the sample [103]. Obviously, if the same area is imaged by selecting an excitation frequency slightly lower than f_1, the contrast is reversed [60, 103]. Such an approach is effective only if low-frequency shifts are involved (i.e., for low variation of the surface elastic properties or near the saturation of the frequency shift, which is obtained for high values of k_s=k_c), whereas too wide shifts produce a contrast in the acoustic image, which is then no longer representative of the mechanical properties of the sample.

The UFM technique can also be used for indentation modulus mapping. In principle, d-UFM measurements of force versus threshold amplitude could be performed at each point of the scanned area, thus obtaining the $k_s(x,y)$ map, which can be subsequently converted into the $M_s(x,y)$ one. Alternatively, while imaging the sample surface in standard constant force, one could acquire at each point of the area the threshold amplitude, which is inversely proportional to the local value of the contact stiffness if the same load is applied and supposing adhesion forces to be constant over the scanned surface (see Fig. 4b) [66]. Finally, the acquired image could be converted into the $k_s(x,y)$ map after calibration through a reference sample.

The most effective approach for mapping the mechanical properties using UFM is that reported by Dinelli et al. [66]: the cantilever deflection signal is analyzed by a lock-in amplifier that extracts the amplitude of its sinusoidal component at the repetition frequency of the ramp signal (namely, A_{UFM}) at each point of the scanned area, thus obtaining the $A_{UFM}(x,y)$ map. A_{UFM} is inversely proportional to the threshold amplitude and, consequently, it is directly proportional to k_s: the contrast in the A_{UFM} images thus quantitatively represents the relative value of E_s^* of the sample surface, as far as the adhesion force is constant over the imaged area. Finally, the $A_{UFM}(x,y)$ map can be converted into the quantitative $M_s(x,y)$ one by proper calibration. To this aim, the $A_{UFM}(x,y)$ map can be converted into the $k_s(x,y)$ one by performing a force versus threshold calibration at a fixed point of the imaged area. Alternatively, A_{UFM} itself can be measured on a reference sample, thus obtaining the proportionality coefficient to directly convert the $A_{UFM}(x,y)$ map into the E_s^* (x,y) one.

Applications

The capability of U-AFM techniques for evaluating the sample elastic modulus has been demonstrated through spot measurements on different stiff bulk samples, either single crystals [65, 99, 101] or amorphous materials [93, 104]. Owing to their high lateral resolution, U-AFM techniques have been used for the qualitative and quantitative mechanical imaging at microscales and nanoscales of a wide number of samples, such as nanocrystalline ferrites [61]; piezoelectric ceramics [103]; biphasic polymer blends [66, 105–107]; polymeric matrices incorporating rubber nanoparticles [108], single crystals [104], glass [66, 102] or carbon [109] fibers, or carbon nanotubes [110]; multiphase metallic materials [111]; and precipitates in polycrystalline matrices [112]. Since a small volume of sample under the tip contributes to the measured contact stiffness, U-AFM techniques are particularly suitable for the elastic characterization of films and coatings. In particular, Hurley et al.

[63, 102, 113–115] demonstrated the reliability of U-AFM elastic measurements by comparing the results obtained via such techniques with those obtained by standard methods, such as SAWs or DSI, on different film samples. U-AFM has been successfully used for the characterization of thin and ultrathin nanocrystalline nickel films [100, 115, 116], diamond-like carbon films [62], niobium films [102], nanosized granular gold films [117], and clay mineral films [118]. Finally, the combination of the aforementioned features, which implies nanometric lateral and vertical dimensions of the probed volume of the sample, makes the techniques described in this review powerful tools for the mechanical characterization of microstructures and nanostructures. U-AFM techniques have recently been used to characterize polymeric nanobundles [119].

Zheng et al. [114] used both the AFAM technique and the UFM technique to characterize tin oxide nanobelts (with width and thickness approximately 900 and 50 nm, respectively) pinned on silicon substrates: fairly good agreement was found by the authors between the values of the indentation modulus of the SnO_2 nanobelts in the (102) crystallographic direction evaluated (approximately 150±15 GPa) by the AFAM technique (with estimated probed depth as high as 45–60 nm) and those evaluated by the d-UFM (with estimated probed depth as high 14–24 nm) technique [95, 114]. Such agreement between the AFAM and UFM results is particularly interesting since it confirms the substantial negligibility of the mechanical properties of the silicon substrate in AFAM measurements [114], although the AFAM-probed depth was comparable with the thickness of the nanobelts. Very recently, Stan et al. [120] used the AFAM technique to characterize tellurium microcrystals and nanowires. The unique capability of the UFM technique of high spatially resolved quantitative mechanical imaging recently allowed Muthaswami et al. [121] to characterize multiwalled carbon nanotubes deposited either by arc discharge or chemical vapor deposition: according to the authors, the mechanical images of the multiwalled carbon nanotubes deposited by chemical vapor deposition reveal a radial nanostructure more highly nonuniform than that observed in the images of the multiwalled carbon nanotubes deposited by arc discharge, with increased defect density [121]. Similar lateral resolution was achieved by Stan et al. [122] using the AFAM technique to characterize aluminum nitride nanotubes. UFM has been also used for the characterization of integrated circuit test structures [96, 123, 124].

Finally, we have to mention the valuable work of Kolosov et al. [68] where germanium nanoislands epitaxially grown on silicon substrates were investigated by UFM: with a lateral resolution of 5–10 nm, the authors observed a variation in the mechanical properties along the cross section of the dots which was compatible with strained germanium dots with relaxed germanium in the center [68]. Such a finding was confirmed by transmission electron microscopy (TEM), thus indicating UFM—and in general U-AFM techniques—is capable in certain cases of supplying, in a nondestructive way, information on the local nanostructure of samples similar to that retrieved by TEM, which is, nevertheless, a highly destructive technique. All such results demonstrate the potential of U-AFM techniques for the characterization of nanostructures and indicate the improvement of the resolution and the reliability at the nanoscale as one of the most challenging issues for the future.

Thin-film applications: substrate effect

In the case of ultrathin films, even AFM measurements may be affected by the mechanical properties of the substrate if the tip-sample contact radius a is not sufficiently lower than the film thickness t_f. Therefore, the "film-only" mechanical properties have to be deduced from those measured on the "film-substrate" system by methods similar to those developed for the analysis of DSI data. The measured indentation modulus M_{meas} is expected to be a function of both the indentation modulus of the film and that of the substrate (M_f and M_{sub}, respectively) and of the ratio a/t_f (or, alternatively, of the ratio h/t_f, where h is the indentation depth) [47]. For $a/t_f << 1$ the elastic response is film-dominated (M_{meas} approaches M_f if $a/t_f \rightarrow 0$), whereas for $a/t_f >> 1$ the response is substrate-dominated (M_{meas} approaches M_s for $a/t_f \rightarrow \infty$). Finally, in the intermediate range a transition is expected between M_f and M_{sub}, the description of which has been extensively addressed in the literature by proposing a wide number of different models [44–47]. After a suitable explicit relation $M_{meas}(M_f, M_{sub}, a/t_f)$ has been assumed, the value of M_f is deduced from that of M_{meas} if the mechanical properties of the substrate, t_f, and a are known. Note that, as far as the latter is concerned, the experimental error in the final value of M_f retrieved by U-AFM techniques is higher than in standard DSI tests, owing to the uncertainty in the tip shape and dimensions. If that mechanical imaging is performed, by repeating this approach at each point of the scanned area, one can deduce the map of the "film-only" indentation modulus $M_f(x,y)$ from that of the as-measured values of the sample indentation modulus $M_{meas}(x,y)$ if the elastic properties of the substrate and the thickness of the film are known. If ultrathin films with high surface roughness are characterized, the local variation in the sample height may be a significant fraction of the whole film thickness and, consequently, the local value of t_f should be used to correctly calculate M_f from M_{meas}. To that aim, the capability of the U-AFM techniques described to retrieve

the indentation modulus map $M_{meas}(x,y)$ simultaneously to the sample morphology is particularly helpful: the average surface height (namely, δ_{mean}) calculated from the morphological image [i.e., the map $\delta(x,y)$] can be assumed to correspond to the film thickness, the latter being previously measured. The map of the local thickness values [namely, $t_f(x,y)$] can thus be deduced as $t_f(x,y) = t_f + \delta(x,y) - \delta_{mean}$ [125]. Finally, $t_f(x,y)$ can be used to locally correct the substrate effect on U-AFM indentation modulus measurements, thus obtaining the "film-only" indentation modulus map $M_f(x,y)$ from $M_{meas}(x,y)$ [125]. As an example of such an approach, Fig. 5a shows the morphological characterization, obtained in AFM standard contact mode, of an aluminum finger deposited on a glass substrate, revealing an almost uniform film thickness t_f=88 nm far from the edge of the finger where huge agglomerates of material are observable. Following the AFAM approach, f_1 and f_2 images were collected (Fig. 5b, c, respectively) and used to solve Eq. 2, thus obtaining the $k_s(x,y)$ map reported in Fig. 5d. The tip was determined to be flat with a radius a= 27 nm, by using the glass substrate region as the reference material and assuming its average indentation modulus was M_{sub}=88 GPa [93], thus obtaining the indentation modulus map $M_{meas}(x,y)$ reported in Fig. 5e. Finally, by using Gao's

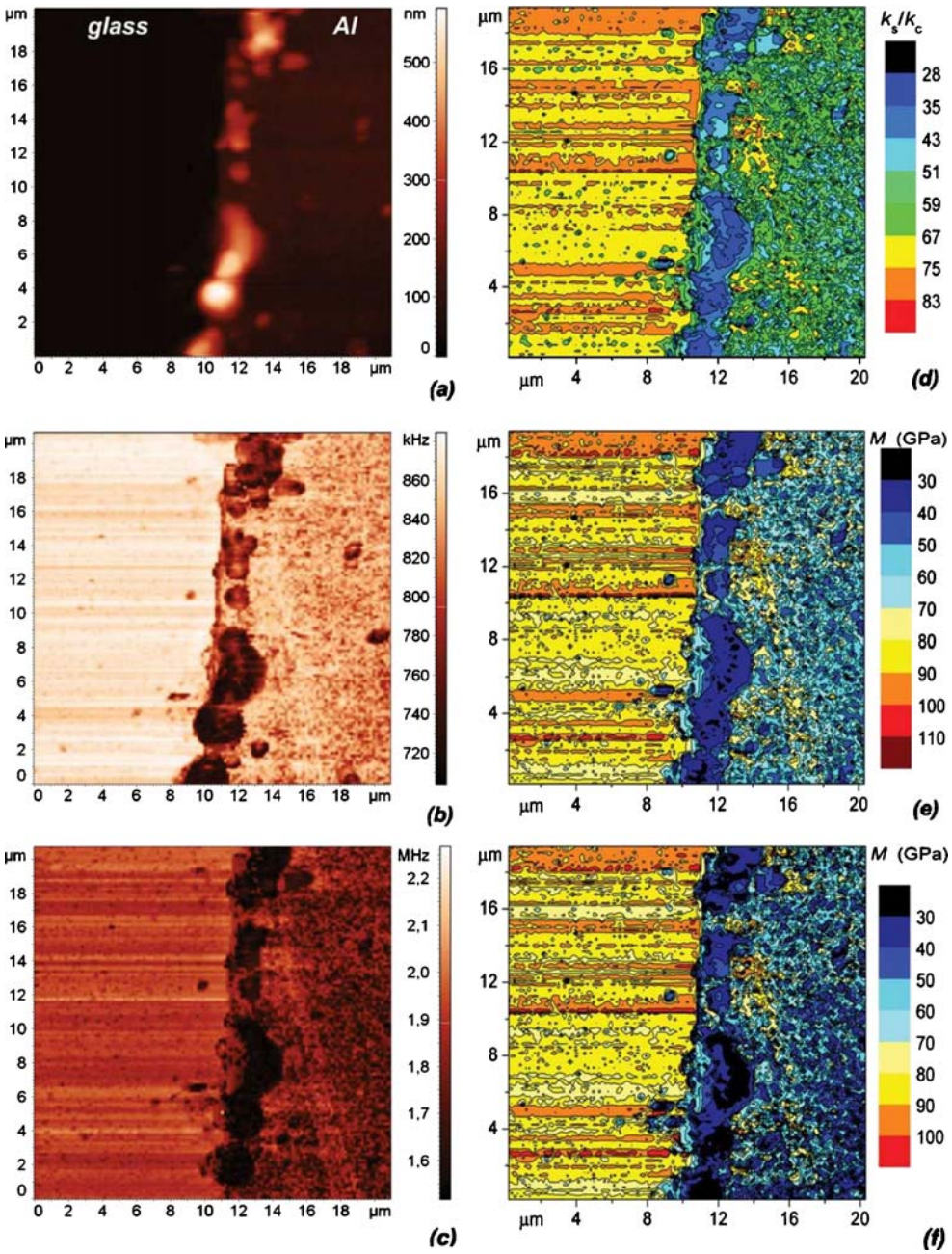

Fig. 5 **a** AFM standard contact mode morphological characterization of an aluminum finger, deposited on a glass substrate, near its edge. **b**, **c** Maps of the first (f_1) and second (f_2) contact resonance frequencies, respectively, obtained using the AFAM approach. **d** Map of the tip-sample contact stiffness k_s normalized with respect to the cantilever spring constant k_c. **e** The as-measured map of the indentation modulus $M_{meas}(x,y)$. **f** Map of the "film-only" indentation modulus $M_f(x,y)$, obtained from $M_{meas}(x,y)$ through Gao's formula, where the local film thickness was evaluated from data reported in **a**

formula [46] at each point of the area and evaluating the local film thickness from Fig. 5a, one retrieves the "film-only" indentation modulus M_f reported in Fig. 5f. The average value of the as-measured indentation modulus of the aluminum film is evaluated as M_{meas}=60 GPa, whereas its average value after correcting for the substrate effect is found to be as high as M_f=53 GPa, which is compatible with data obtained by DSI measurements reported in the literature [126, 127].

Other properties affecting the stiffness

Although the $k_s(x,y)$ map is primarily the characterization of the local elastic modulus, a number of factors affect the value of k_s, resulting in an apparent inhomogeneity of the elastic properties of the sample surface. The roughness of the surface is responsible for local variation of the contact area A_c, which results in an increase or decrease of k_s also for a constant value of M_s, and thus in the apparent stiffening or softening (when A_c increases or decreases, respectively) [95, 121, 128]. Moreover, Hurley and Turner [129] demonstrated that the frequency shift in the AFAM technique is sensitive to variation of the room humidity, which affects the damping coefficient γ_s: neglecting the damping in the AFAM model produces an increase of the apparent contact stiffness corresponding of the increase of the room humidity [129]. Furthermore, Hurley et al. [130] demonstrated that AFAM imaging enables one to differentiate between hydrophilic and hydrophobic surfaces by characterizing 2–3-nm-thick *n*-octyldimethylchlorosilane self-assembled monolayers on silicon substrates, with different surface energy controlled through ultraviolet ozonolysis. Variations in the room humidity were observed to modify the contrast in AFAM images between the silicon substrates and the hydrophilic samples, the latter appearing stiffer as the humidity increased [130]. Conversely, humidity variations do not affect AFAM images of hydrophobic surfaces [130]. U-AFM techniques allow the measurement of the "local" value of k_s which results from the probing of a volume of the sample that depends on the contact radius (generally, it is assumed that the measurement of k_s is affected by the sample down to $3a$ from the surface) [131]. Consequently, if the sample is not homogeneous in such a volume, it results in a variation of the measured value of k_s. In particular, it has been recently demonstrated, with excellent quantitative agreement between simulations and experiments, that the apparent value of k_s is reduced by the presence of subsurface defects and voids [132, 133] as well as by weak adhesion between a film and a buried interface [131].

The latter capability was demonstrated by Hurley et al. by imaging the surface of a test sample constituted by a 20-nm-thick gold film deposited on a silicon single-crystal substrate patterned with a titanium-gold bilayer (each layer 1 nm thick). The apparent contact stiffness, evaluated using the AFAM method, of the region without the titanium interlayer was 5% lower than that of the region with the titanium interlayer. Such a finding cannot be attributed to the variation in the elastic modulus due to the titanium layer, which conversely would have reduced the overall indentation modulus, being more compliant than silicon, but has to be ascribed to the weak adhesion at the buried gold-silicon interface which is improved by the presence of the titanium interlayer [131]. Finally, U-AFM techniques have been demonstrated that allow one to detect subsurface features, such as cracks or dislocations [67, 134–136]. Concerning the latter issue, Yamanaka [135] firstly used the UFM technique for imaging subsurface lattice defects in highly oriented pyrolytic graphite, and observed that acoustic microscopy can nondestructively supply information on subsurface nanoscale crystalline defects, which would otherwise be retrievable only by TEM, which nevertheless require irreversible modification of the sample. Such results were successively confirmed, using the AFAM technique on highly oriented pyrolytic graphite , by Tsuji and Yamanaka [136]: in their work, the authors demonstrated not only the capability of imaging subsurface dislocations, but also the possibility of obtaining reversible lateral motion of subsurface dislocations by varying the load applied on the surface by the tip.

Conclusions

In conclusion, we have given an overview of some ultrasonics-based methods for the characterization of mechanical properties of thin films. Acoustic microscopy was first described. Then, U-AFM techniques were illustrated; these allow qualitative and quantitative determination of elastic properties of the sample surface. Such techniques also allow one to image the presence of subsurface defects, voids, dislocations, and variation of adhesion at buried interfaces.

References

1. Fu Y, Du H, Huang W, Zhang S, Hu M (2004) Sens Actuators A Phys 112:395
2. Dawar AL, Joshi JC (1984) J Mater Sci 19:1
3. Dimitrakopoulos CD, Malenfant PRL (2002) Adv Mater 14:99
4. Haertling GH (1991) J Vac Sci Technol A 9:414
5. Dawber M, Rabe KM, Scott JF (2005) Rev Mod Phys 77:1083
6. Setter N et al (2006) J Appl Phys 100:051606
7. Lettington AH (1998) Carbon 36:555
8. Mabeck JT, Malliaras GG (2006) Anal Bioanal Chem 384:343

9. Bartic C, Borghs G (2006) Anal Bioanal Chem 384:354
10. Rack PD, Holloway PH (1998) Mater Sci Eng R21:171
11. Chopra KL, Paulson PD, Dutta V (2004) Prog Photovolt Res Appl 12:69
12. Tsai HC, Bogy DB (1987) J Vac Sci Technol A 5:3287
13. Kato K (2000) Wear 241:151
14. Gray JE, Luan B (2002) J Alloy Compd 336:88
15. Zhang S, Sun D, Fu Y, Du H (2003) Surf Coat Technol 167:113
16. Hauert R (2003) Diamond Relat Mater 12:583
17. Spaepen F (2000) Acta Mater 48:31
18. Volinsky AA, Moody NR, Gerberich WW (2002) Acta Mater 50:441
19. Vinci RP, Gross D (1996) Annu Rev Mater Sci 26:431
20. Bhushan B, Li X (2003) Int Mater Rev 48:125
21. Krautkrämer J, Krautkrämer H (1983) Ultrasonic testing of materials. Springer, Berlin
22. Lin KH et al (2006) Appl Phys Lett 89:043106
23. Hurley DC, Tewary VK, Richards AJ (2001) Meas Sci Technol 12:1486
24. Wu TT, Chen YY, Huang GT, Chang PZ (2005) J Appl Phys 97:073510
25. Côte R, Van der Donck T, Celis JP, Glorieux C (2009) Thin Solid Films 517:2697
26. Quate CF (1985) Phys Today 34:34
27. Briggs A (1992) Acoustic microscopy. Oxford University Press, New York
28. Maev RG (2008) Acoustic microscopy - fundamentals and applications. Wiley, Weinheim
29. Fischer-Cripps AC (2000) Vacuum 58:569
30. Li X, Bhushan B (2002) Mater Charact 48:11
31. White CC, Vanlandingham MR, Drzal PL, Chang NK, Chang SH (2005) J Polym Sci B Polym Phys 43:1794
32. Fischer-Cripps AC (2006) Surf Coat Technol 200:4153
33. Vlassak JJ, Ciavarella M, Barber JR, Wang X (2003) J Mech Phys Solids 51:1701
34. White CC, Vanlandingham MR, Drzal PL, Chang NK, Chang SH (2005) J Polym Sci B Polym Phys 43:1812
35. Syed Asif SA, Wahl KJ, Colton RJ (1999) Rev Sci Instrum 70:2408
36. Syed Asif SA, Wahl KJ, Colton RJ, Warren OL (2001) J Appl Phys 90:1192
37. Sneddon IN (1965) Int J Eng Sci 3:47
38. Pharr GM, Oliver WC, Brotzen FR (1992) J Mater Res 7:613
39. Oliver WC, Pharr GM (2004) J Mater Res 19:3
40. Oliver WC, Pharr GM (1992) J Mater Res 7:1564
41. Ciavarella M (1999) Int J Solids Struct 36:4149
42. Ngan AHW, Wang HT, Tang B, Sze KY (2005) Int J Solids Struct 42:1831
43. Gao YF, Xu HT, Oliver WC, Pharr GM (2008) J Mech Phys Solids 56:402
44. King RB (1987) Int J Solids Struct 23:1657
45. Bhattacharya AK, Nix WD (1988) Int J Solids Struct 24:1287
46. Gao H, Chiu CH, Lee J (1992) Int J Solids Struct 29:2471
47. Jung YG, Lawn BR, Martyniuk M, Huang H, Hu XZ (2004) J Mater Res 19:3076
48. Buckle H (1973) In: Westbrook JW, Conrad H (eds) The science of hardness testing and its research applications. American Society for Metals, Metals Park, pp 453–491
49. Clifford CA, Seah MP (2005) Appl Surf Sci 252:1915
50. Maivald P et al (1991) Nanotechnology 2:103
51. Nie HY, Motomatsu M, Mizutani W, Tokumoto H (1996) Thin Solid Films 273:143
52. Mazeran PE, Loubet JL (1999) Tribol Lett 7:199
53. Diebold AC (2005) Science 310:61
54. Shekhawat GS, Dravid VP (2005) Science 310:89
55. Burnham NA, Kulik AJ, Gremaud G, Gallo PJ, Oulevey F (1996) J Vac Sci Technol B 14:794
56. Oulevey F et al (1998) Rev Sci Instrum 69:2085
57. Dupas E, Gremaud G, Kulik AJ, Loubet JL (2001) Rev Sci Instrum 72:3891
58. Rabe U, Janser J, Arnold W (1996) Rev Sci Instrum 67:3281
59. Rabe U et al (2002) Surf Interface Anal 33:65
60. Rabe U et al (2000) Ultrasonics 38:430
61. Kester E, Rabe U, Presmanes L, Tailhades P, Arnold W (2000) J Phys Chem Solids 61:1275
62. Amelio S et al (2001) Thin Solid Films 392:75
63. Hurley DC, Shen K, Jennett NM, Turner JA (2003) J Appl Phys 94:2347
64. Kolosov O, Yamanaka K (1993) Jpn J Appl Phys Part 2 32: L1095
65. Dinelli F, Biswas SK, Briggs GAD, Kolosov O (2000) Phys Rev B 61:13995
66. Dinelli F, Assender HE, Takeda N, Briggs GAD, Kolosov OV (1999) Surf Interface Anal 27:562
67. Yamanaka K, Ogiso H, Kolosov OV (1994) Appl Phys Lett 64:178
68. Kolosov OV et al (1998) Phys Rev Lett 81:1046
69. Parmon W, Bertoni HL (1979) Electron Lett 15:684
70. Richard P, Gremaud G, Kulik A (1999) In: Levy M, Schneider SC, McAvoy BR (eds) Proceedings of the 1994 IEEE ultrasonics symposium. IEEE, Piscataway, p 1425
71. Kushibiki J, Chubachi N (1985) IEEE Trans Sonics Ultrason SU-33:189
72. Achenbach JD, Kim JO, Lee Y (1995) In: Briggs A (ed) Advances in acoustic microscopy, vol 1. Plenum, New York, pp 153–208
73. Sklar Z, Mutti P, Stoodley NC, Briggs GAD (1995) In: Briggs A (ed) Advances in acoustic microscopy, vol 1. Plenum, New York, pp 209–247
74. Banerjee S, Gayathri N, Dash S, Tyagi AK, Raj B (2005) Appl Phys Lett 86:211913
75. Yamanaka K, Nakano S (1996) Jpn J Appl Phys Part 1 35:3787
76. Cuberes MT, Briggs GAD, Kolosov OV (2001) Nanotechnology 12:53
77. Schwarz K, Rabe U, Hirsekorn S, Arnold W (2008) Appl Phys Lett 92:183105
78. Rabe U et al (2007) Nanotechnology 18:044008
79. Tsuji T, Irihama H, Yamanaka K (2002) Jpn J Appl Phys Part 1 41:832
80. Kos AB, Hurley DC (2008) Meas Sci Technol 19:015504
81. Rabe U, Kester E, Arnold W (1999) Surf Interface Anal 27:386
82. Reinstaedtler M, Rabe U, Scherer V, Turner JA, Arnold W (2003) Surf Sci 532:1152
83. Turner JA, Wiehn JS (2001) Nanotechnology 12:322
84. Mahdavi MH, Farshidianfar A, Tahani M, Mahdavi S, Dalir H (2008) Ultramicroscopy 109:54
85. Yuya PA, Hurley DC, Turner JA (2008) J Appl Phys 104:074916
86. Shen K, Hurley DC, Turner JA (2004) Nanotechnology 15:1582
87. Lee HL, Yang YC, Chang WJ, Chu SS (2006) Jpn J Appl Phys 45:6017
88. Rabe U, Turner J, Arnold W (1998) Appl Phys A 66:S277
89. Senden TJ, Ducker WA (1994) Langmuir 10:1003
90. Cleveland JP, Manne S, Bocek D, Hansma PK (1993) Rev Sci Instrum 64:403
91. Sader JE, Chon JWM, Mulvaney P (1999) Rev Sci Instrum 70:3967
92. Passeri D (2007) Tecniche non distruttive di caratterizzazione meccanica ed elettromeccanica di materiali dalla scala macroscopica a quella nanoscopica. PhD thesis, University of Rome "La Sapienza"

93. Hurley DC, Turner JA (2007) J Appl Phys 102:033509
94. Weisenhorn AL, Khorsandi M, Kasas S, Gotzos V, Butt HJ (1993) Nanotechnology 4:106
95. Zheng Y, Geer RE, Dovidenko K, Kopycinska-Müller M, Hurley DC (2006) J Appl Phys 100:124308
96. Muthuswami L, Moyer ES, Li Z, Geer RE (2002) In: Interconnect technology conference, 2002. Proceedings of the IEEE 2002 international, pp 239–241. doi:10.1109/IITC.2002.1014945
97. Bykov V, Gologanov A, Shevyakov V (1998) Appl Phys A 66:499
98. Kopycinska-Müller M, Geiss RH, Hurley DC (2006) Ultramicroscopy 106:466
99. Passeri D et al (2005) Rev Sci Instrum 76:093904
100. Kopycinska-Müller M et al (2008) Z Phys Chem 222:471
101. Stan G, Price W (2006) Rev Sci Instrum 77:103707
102. Hurley DC, Kopycinska-Müller M, Kos AB, Geiss RH (2005) Adv Eng Mater 7:713
103. Rabe U et al (2002) J Phys D 35:2621
104. Passeri D et al (2007) Microelectron Eng 84:490
105. Rabe U, Scherer V, Hirsekorn S, Arnold W (1997) J Vac Sci Technol B 15:1506
106. Bliznyuk VN et al (2007) Langmuir 23:12973
107. Marinello F, Schiavuta P, Vezzu S, Patelli A, Carmignato S, Savio E (2009) In: 12th international conference on metrology and properties of engineering surfaces, 8–10 July, Rzeszów, Poland
108. Porfyrakis K, Kolosov OV, Assender HE (2001) J Appl Polym Sci 82:2790
109. Yamanaka K, Maruyama Y, Tsuji T, Nakamoto K (2001) Appl Phys Lett 78:1939
110. Passeri D et al (2008) Physica E 40:2419
111. Kumar A, Rabe U, Arnold W (2008) Jpn J Appl Phys 47:6077
112. Kumar A, Rabe U, Hirsekorn S, Arnold W (2008) Appl Phys Lett 92:183106
113. Hurley DC, Kopycinska-Müller M, Kos AB, Geiss RH (2005) Meas Sci Technol 16:2167
114. Hurley DC, Kopycinska-Müller M, Kos AB (2007) JOM 59:23
115. Hurley DC et al (2005) J Mater Res 20:1186
116. Passeri D et al (2006) Appl Phys Lett 88:121910
117. Stan G, Cook RF (2008) Nanotechnology 19:235701
118. Prasad M, Kopycinska M, Rabe U, Arnold W (2002) Geophys Res Lett 29:1172
119. Iwate F, Matsumoto T, Sasaki A (2000) Nanotechnology 11:10
120. Stan G et al (2009) Ultramicroscopy 109:929
121. Muthaswami L et al (2007) Nano Lett 7:3891
122. Stan G et al (2009) Nanotechnology 20:035706
123. Muthaswami L, Geer RE (2004) Appl Phys Lett 84:5082
124. Geer RE, Kolosov OV, Briggs GAD, Shekhawat GS (2002) J Appl Phys 91:4549
125. Passeri D et al (2008) Superlattices Microstruct 44:641
126. Chinmulgund M, Inturi RB, Barnard JA (1995) Thin Solid Films 270:260
127. Lim YY, Chaudhri MM, Enomoto Y (1999) J Mater Res 14:2314
128. Muraoka M (2005) Nanotechnology 16:542
129. Hurley DC, Turner JA (2004) J Appl Phys 95:2403
130. Hurley DC, Kopycinska-Müller M, Julthongpiput D, Fasolka MJ (2006) Appl Surf Sci 253:1274
131. Hurley DC, Kopycinska-Müller M, Langlois ED, Barbosa N III (2006) Appl Phys Lett 89:021911
132. Sarioglu AF, Atalar A, Degertekin FL (2004) Appl Phys Lett 84:5368
133. Parlak Z, Degertekin FL (2008) J Appl Phys 103:114910
134. McGuigan AP et al (2002) Appl Phys Lett 80:1180
135. Yamanaka K (1996) Thin Solid Films 273:116
136. Tsuji T, Yamanaka K (2001) Nanotechnology 12:301